Improving optical transmission of spark-plasma-sintered yag ceramics

Boilet, L.; Aubry, P.; Henrard, Luc; Deparis, Olivier; Palmero, P.; Lardot, V.; Cambier, F.; Moronta Perez, Rosa

Published in:
Journal of Ceramic Science and Technology

DOI:
10.4416/JCST2017-00052

Publication date:
2018

Document Version
Peer reviewed version

Journal of
Ceramic Science
and Technology

J. Ceram. Sci. Technol., **09** [1] 19-28 (2018)
DOI: 10.4416/JCST2017-00052
available online at: http://www.ceramic-science.com

Improving Optical Transmission of Spark-Plasma-Sintered YAG Ceramics: Effect of Powder Conditioning and Post-Treatments

R. Moronta Pérez*[1], L. Boilet[1], P. Aubry[1], P. Palmero[2], L. Henrard[3], O. Deparis[3], V. Lardot[1], F. Cambier[1]

[1]Belgian Ceramic Research Centre, 4 avenue gouverneur Cornez, 7000 Mons (Belgium)
[2]Department of Applied Science and Technology and INSTM Research Unit PoliTO, LINCE Laboratory, Politecnico di Torino, 24 corso Duca degli Abruzzi, 10129 Torino (Italy)
[3]University of Namur, Physics Department, 61 rue de Bruxelles, 5000 Namur (Belgium)
received July 7, 2017; received in revised form September 11, 2017; accepted October 13, 2017

Abstract

Three YAG powders were densified by means of spark plasma sintering (SPS), with the aim of developing optically transparent ceramics. The influence of the physico-chemical characteristics of the powders (purity, agglomeration state and stoichiometry) on the sintering and the optical transmission was investigated. Depending on the powder type, different pre-treatments and/or post-treatments were necessary to increase both homogeneity and optical transmission of the densified parts. In the case of agglomerated powders, dispersion by ultrasonication was efficient and led to better homogeneity and higher optical transmission. Post-treatments such as annealing and post-hipping in air were helpful to reduce oxygen vacancies and residual porosities and improved the optical transmission of the ceramics. The highest values of real in-line transmission (RIT) were obtained under SPS conditions of 50 MPa at 1500 °C and after annealing in air at 1150 °C for 12 h. The achieved RIT value was equal to 66 % at the wavelength of 600 nm.

Keywords: YAG, SPS, transparent ceramics, optical properties

I. Introduction

Transparent polycrystalline ceramics combine good optical properties and, compared to single crystals, higher mechanical properties and low manufacturing costs. However, processing conditions leading to transparency are very narrow and a combination of different parameters must be taken into account in order to maximize optical transparency. Generally speaking, the concentration of defects in the ceramics must be as low as possible. Defects may be impurities, secondary phases or residual porosity. In fact, impurities or secondary phases scatter and absorb light and, consequently, decrease the in-line optical transmission. Moreover, pores, with a refractive index different from that of the ceramic material, also scatter light, so that transparency can only be achieved for ceramics with full density. In addition to numerous technical challenges to obtain transparent ceramics, comprehensive studies are limited owing to the expense of high-purity commercial powders.

Spark plasma sintering (SPS) combines uniaxial pressure and heating based on the Joule effect, and offers the possibility of sintering powders up to full density at lower temperatures compared to conventional sintering. In recent years, various transparent ceramics have been obtained with SPS: $MgAl_2O_4$ [1, 2, 3], YAG [4, 5, 6], Al_2O_3 [7, 8], MgO [9] and $BaTiO_3$ [10], for example. However, inhomogeneity and colouring of transparent ceramics often appears after sintering and decreases the optical transmission in the visible range. These defects may come from the starting powder (impurities [11] or high level of agglomeration [12, 13]), as well as from the sintering process (graphite contamination [14], oxygen vacancies owing to reducing atmosphere during sintering [15, 16] or presence of residual porosities [17]). Several attempts have been made to improve the optical transmission of ceramics by powder milling [18], addition of sintering aids like LiF or MgO [19, 20], post-annealing [18] or modification of the sintering cycle [7, 21, 22]. However, the respective influences of powder characteristics and sintering conditions (effect of heating rate, temperature, pressure and pressure schedule) on the inhomogeneity of samples are not clearly understood.

YAG ($Y_3Al_5O_{12}$) is one of the most widely used transparent ceramics. The applications of doped YAG as laser and scintillation material are well-known [23, 24, 25], and thanks to its high strength and hardness it is also suitable as a structural ceramic [26].

In this work, three different YAG powders are studied for comparison: one powder synthesized under laboratory conditions by means of co-precipitation (YAG-S) and two commercially available powders coming from different synthesis routes: YAG-B, based on sulphate precursors, and YAG-N prepared by means of flame spray py-

* Corresponding author: r.morontaperez@bcrc.be

rolysis. First, the influence of the SPS parameters on the densification and microstructure of the sintered parts is discussed and related to the physico-chemical properties of the three powders. Then, according to these results, for each powder, adapted attempts are tested to increase the optical transmission: dispersion, air annealing and/or LiF addition.

The influence of the powders' purity level is highlighted and the effects of pre- and post-treatments on the optical properties are assessed. Two different optical measurements (respectively, real in-line transmission and total forward transmission) are carried out in order to quantify the amount of light scattered in the obtained transparent/translucent samples.

II. Experimental

(1) Materials and methods

Three different YAG powders were used in this study: two commercial powders (Baikowski (F) and Nanocerox Inc (USA), hereafter called YAG-B and YAG-N, respectively) and a home-synthesized powder (YAG-S). The latter was synthesized following a reverse-strike coprecipitation route, starting from a mixed aqueous solution of yttrium and aluminium chlorides. The complete procedure is described extensively elsewhere [18, 27]. Briefly, an aqueous solution of chlorides was added drop-wise into an aqueous solution of ammonium hydrogen carbonate, under mild agitation at room temperature. The slurry was aged for 24 h and then washed by means of centrifugation several times in distilled water and in ethanol. Finally, the slurry was dried for 24 h in an oven at 70 °C, resulting in a soft cake, easily crushed in an agate mortar. The resulting powder was calcined at 1000 °C, the minimum temperature required to obtain pure YAG phase. Commercial LiF (99.98 %, Acros Organics) was used as a sintering additive in some YAG samples. The YAG and LiF powders' characteristics were measured and are presented in Table 1. They are compared later in the discussion section.

The powders were dispersed in water with a 19-mm-diameter ultrasonic probe Sonics Vibra-cell and then the suspension obtained was placed in a freeze dryer (HETO, FD8 – 55) for 24 h. The powders were pre-compacted (30 MPa) into a graphite die of 20 mm inner diameter and consolidated by means of spark plasma sintering (HPD10, FCT, Germany) under low vacuum (10 Pa). In order to compare the different assays easily, recorded shrinkage data were transformed into relative density values, taking into account thermal expansion of both the sample and the graphite tools. However, data were recorded only from 500 °C owing to the pyrometer used. To complete densification of the samples, some pre-sintered samples underwent hot isostatic pressing (HIP). Experiments were performed in a GPS VITEK HIP equipped with a platinum furnace, under Ar/O_2 atmosphere (80/20 vol%). The cycle was a heating rate of 5 K/min up to 1250 °C and isostatic pressure of 120 MPa for 1 h.

(2) Characterization

Phase compositions were identified with X-ray diffraction (Miniflex 600 Rigaku) operating with CuKα radiation (1.541874 Å). Diffractograms were recorded at 2θ values ranging from 20 to 90°. A semi-quantitative phase analysis was performed, taking into account the relative peaks intensities, using the reference intensity ratio (RIR) method. The specific surface area of the powders was analysed with a Micromeritics FlowSorb III 2310 at 77 K with N_2 as adsorbate gas. Trace-level elemental analysis was performed using inductively coupled plasma optical emission spectrometry (ICP-OES VARIAN 720-ES) and X-ray photoelectron spectroscopy (XPS K-ALPHA, ThermoFisher Scientific). Agglomerate size distribution between 0.01 and 2000 μm was acquired with a laser particle size analyser (Malvern Mastersizer 2000, UK), using water as the dispersion medium. Densities of all samples were measured by means of water immersion. The theoretical density of 4.553 $g \cdot cm^{-3}$ was used to evaluate the relative density. The uncertainty of the measured density was estimated in ± 0.1 % in our samples.

For evaluating the microstructure, sintered samples were mirror-polished with a diamond paste down to 1 μm and then thermally etched in air at 100 °C below the sintering temperature. Powders and microstructures were observed with a field-emission scanning electron microscope (JEOL 7500F) equipped with a JED 2300 microanalysis system for elemental analysis.

The optical transmittance spectrum of the samples was measured within the wavelength region of 300 – 900 nm using a double-beam UV-visible spectrophotometer (Perkin-Elmer Lambda 750S) and the results were extrapolated, following the Beer-Lambert law, to a thickness of 1 mm using the following equation [11]:

$$T = T_{lim} \cdot \left(\frac{T_s}{T_{lim}} \right)^{(d/d_s)}$$

where T is the transmission normalized at 1 mm thickness, T_{lim} is equal to 84 %, (i.e. the maximal transmission of a perfect YAG material, calculated from the Fresnel formula considering a mean refractive index of 1.82 in the visible range), T_s is the measured transmission of the sample, d and ds are the 1-mm normalized thickness and the sample thickness, respectively. Real-in-line transmission (RIT) and total-forward-transmission (TFT) were both recorded. For TFT measurements, the sample is placed close to the detector, which collects all the light going through the sample, that is both in-line transmitted and scattered light. In contrast, for RIT measurements, sample is situated ~ 1 m away from the detector, which collects only the light transmitted in a very narrow angle, avoiding the scattered light [28].

III. Results and Discussion

(1) Powders analysis and SPS dilatometric comparison

The powder characteristics are summarized in Table 1. XRD measurement on the home-synthesized powder shows that YAG-S contains pure YAG phase. In contrast, the two commercial powders present a mixture of different phases: 96 % YAG, with YAP ($YAlO_3$) and YAM ($Y_4Al_2O_9$) for YAG-B, and mainly hexagonal $YAlO_3$ (90 wt%) with only a very small quantity of YAG phase (around 7 wt%), for YAG-N. The YAG-B powder

Table 1: Characteristics of the starting powders.

	Phases detected by XRD	SSA (m^2/g)	Primary particle size (nm), SEM observations	Powders impurities, > 10 ppm, measured by ICP
YAG - B	YAG (96%) + YAM + Y_2O_3	7 ± 0.1	~ 200	S: 500 ± 10 ppm
YAG - S	YAG	46 ± 0.2	< 100	-
YAG - N	h-$YAlO_3$ (90%) + YAG + YAM	20 ± 0.2	< 200	-
LiF	LiF	*	< 2000	-

SSA: specific surface area; *not measured

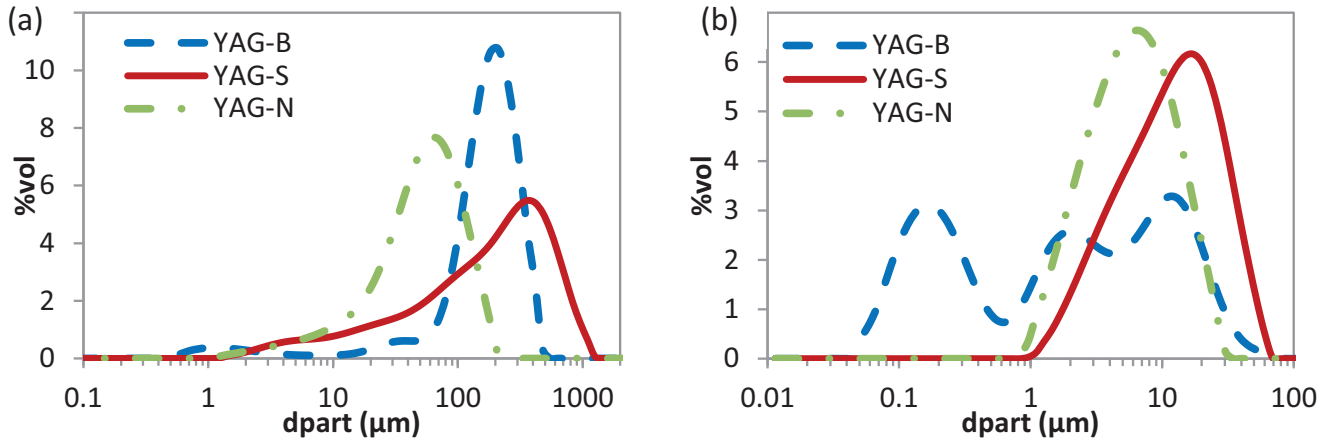

Fig. 1: Frequency distribution (vol%) versus particle size of YAG-B, YAG-S and YAG-N (a) as-received and (b) after 5 min weak US dispersion.

presents a non-negligible amount of sulphur coming from the synthesis route. No impurities were detected in YAG-S and YAG-N.

Fig. 1a shows that, despite a small primary particle size (see Table 1), both YAG-B and YAG-S powders are composed of agglomerates with a large size distribution. Even after weak dispersion by ultrasonication (US) inside the laser granulometer, this distribution remains large and agglomerates of around 70 µm are still measured (Fig. 1b). As received, the YAG-N powder also presents a relatively large particle size distribution (Fig. 1a). Nevertheless, these agglomerates seem softer than those in YAG-B or YAG-S owing to the decrease in the powder's particle size distribution after weak ultrasonication.

The sintering behaviour of the three YAG powders was evaluated by measuring the thermal expansion in the SPS equipment at a heating rate of 20 K/min from 500 to 1650 °C under a pressure of 50 MPa applied during the whole sintering cycle. Results are reported in Fig. 2. Owing to its higher surface area, the green density of YAG-S (30 %) is much lower than that of YAG-N (41 %) and YAG-B (53 %). However, YAG-S powder is more reactive, showing a lower onset sintering temperature (900 °C vs. 1150 °C) and reaching also nearly full density at a lower temperature (1350 °C vs. 1450 – 1500 °C for the two other YAG powders). The sintered samples exhibit a dark appearance. XRD semi-quantitative analyses show that after SPS at 1650 °C, YAG-S and YAG-N samples are composed of pure YAG phase, while YAG-B presents traces of YAP ($YAlO_3$) and YAM ($Y_4Al_2O_9$) (< 0.5 wt%).

In a comparison of the sintering curves of YAG-B and YAG-N, both powders show similar behaviour. Nevertheless, three main differences appear. First, the relative density of YAG-N is 41 % at 500 °C, lower than YAG-B, according to its specific surface (20 vs. 7 m^2/g) and agglomerate size distribution. YAG-B presents a multimodal agglomerate size distribution and should lead to a higher green density. Second, there is a slope change between 900 and 1050 °C corresponding to the transformation of h-$YAlO_3$ and YAM into the YAG phase [29]. This difference is noticeable owing to the large amount of h-$YAlO_3$ in YAG-N powder. Third, this powder is slightly more reactive than YAG-B, and reaches full density at 1450 °C (vs. 1500 °C for YAG-B). This behaviour fits with its surface area too. XRD analysis shows that, at 1650 °C, unlike YAG-B, YAG-N consists of pure YAG phase, so all the intermediate phases have completely evolved to YAG.

(2) SPS parameters' influence on densification and optical transmission

The effect of sintering temperature was studied on the YAG powders. The SPS cycles were as follows: a first rapid heating step at 100 K/min up to 1100 °C, followed by a slower step at a heating rate of 10 K/min up to the final temperature, followed by a 15-min-long isothermal step. The pressure (50 MPa) was applied before heating. Fig. 3 shows images of the sintered samples, related microstructure and final density for the three powders.

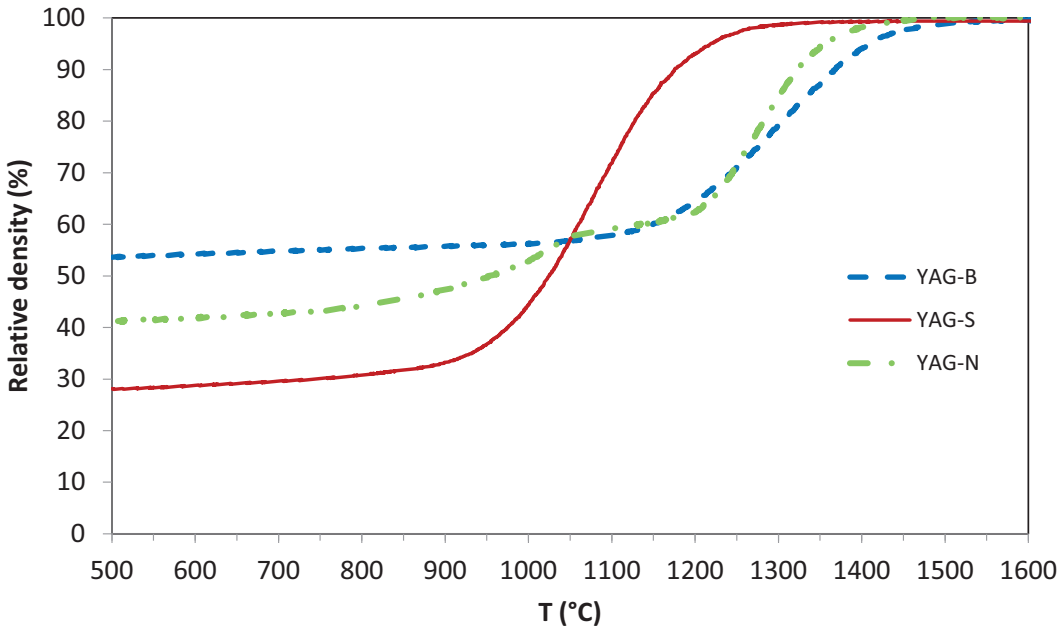

Fig. 2: Relative density of YAG-B, YAG-S and YAG-N powders as a function of the temperature.

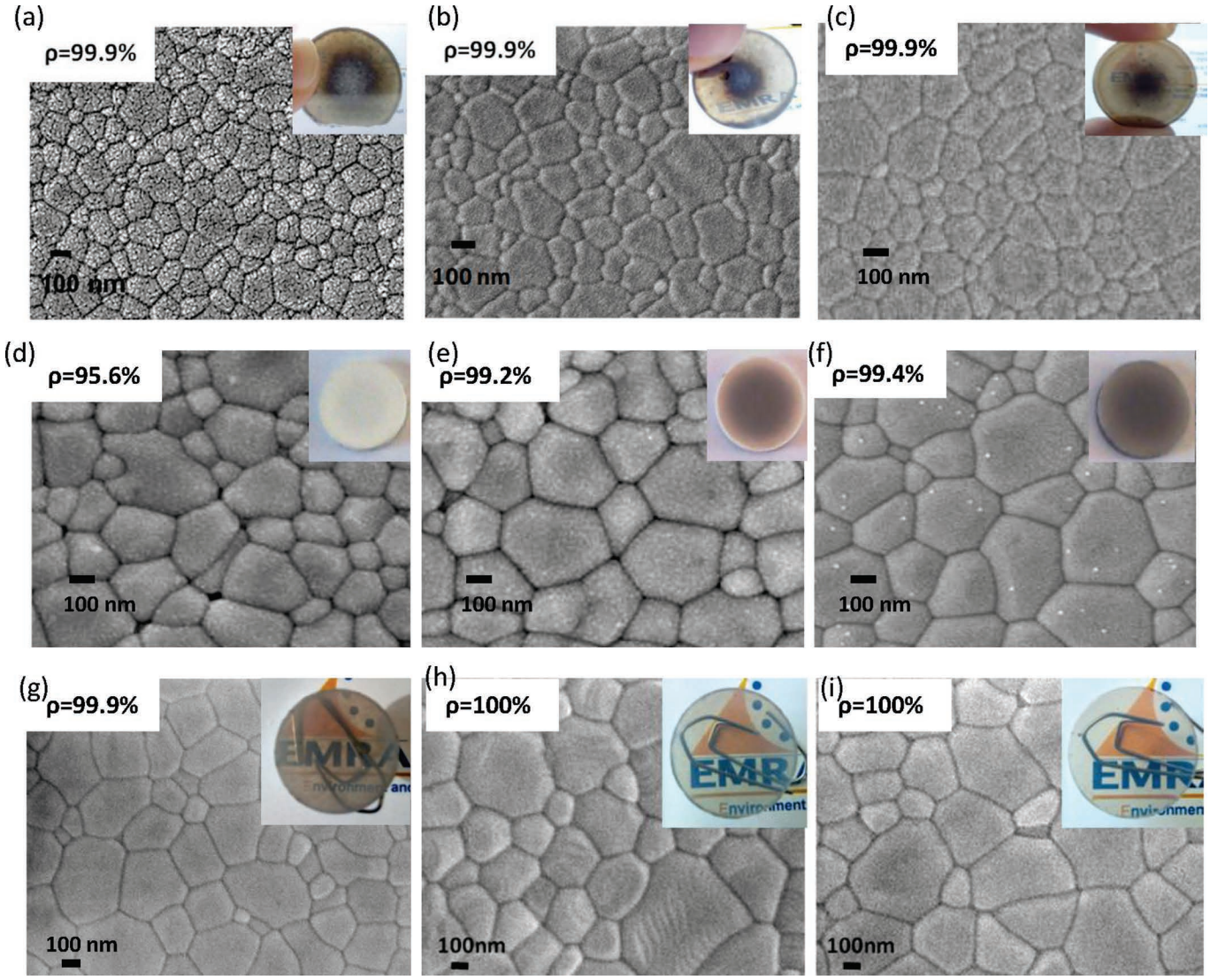

Fig. 3: Scanning electron micrographs of YAG-S sintered at 1200 °C (a), 1250 °C (b) and 1300 °C (c); YAG-B sintered at 1350 °C (d), 1400 °C (e) and 1450 °C (f) and YAG-N sintered at 1400 °C (g), 1450 °C (h) and 1500 °C (i).

YAG-S samples reached almost full densification for all tested temperatures (between 1200 and 1300 °C) and only the YAG phase was detected with XRD. The presence of pure YAG in the final samples implies a high homogeneity of the distribution of Y and Al cations in the as-synthesised product. However, the samples showed a core-shell aspect, with an opaque central part (hereafter denoted as the core or centre) and a more transparent outer part. At temperatures higher than 1300 °C, the opaque centre diminished but, unfortunately, so did the optical transmission of the outer part. At microstructural level, the grain size increases slightly between 1200 and 1300 °C, reaching values around 200 nm at 1300 °C. As no difference in terms of residual porosity and grain size is observed between the peripheral part and the centre of the samples, this core-shell aspect cannot be attributed to a thermal gradient during sintering.

In the case of YAG-B, SEM micrographs show a decrease of intergranular porosity and slight grain growth with the increase of the sintering temperature. At 1450 °C, relative density reaches 99.4 % and the mean grain size is around 400 nm. In addition, an increasing darkening of the samples with increasing temperature and density can be observed. Table 2 shows the evolution of YAG-B composition as a function of the sintering temperature. Higher temperatures lead to a decrease of secondary phase content (YAP and YAM) in favour of YAG phase. According to the Al_2O_3/Y_2O_3 phase diagram, the transformation of YAP and YAM phases into YAG implies the presence of alumina in the starting powder. However, XRD analyses did not reveal the presence of alumina phases: either these phases are amorphous or their content is lower than the instrumental detection limit. Concerning impurities, we have observed a decrease of the sulphur content after SPS and with the temperature. In samples sintered in SPS at 1450 °C, only 150 ppm sulphur has been detected. The residual presence of sulphur may inhibit both densification and phase transformation into pure YAG (which is incomplete even at 1450 °C, much higher than the YAG temperature formation). Presence of YAM, YAP or Y_2O_3 phases in the sintered ceramics may also be due to the sintering process, SPS, with thermal cycles too rapid to allow complete reactions into pure YAG.

Table 2: Evolution of the phase composition on YAG-B as a function of the sintering temperature (pressure is 50 MPa, dwell time 15 minutes). XRD semi-quantitative analysis, in wt%.

	% YAG	% YAM	% YAP
1350 °C	96.5	1.5	2.0
1400 °C	96.8	0.2	3.0
1450 °C	98.9	0.3	0.8

Fig. 3 shows also YAG-N samples sintered between 1400 and 1500 °C. At temperatures lower than 1400 °C, the samples showed some intergranular porosity and were not completely transparent. From 1450 °C, transparent samples, with grain size between 200 and 800 nm, are obtained. They present a slight darkening after SPS but less noticeable than in the other two powders. The relative density measured in all cases was close to 100 % and XRD measurement showed only YAG phase. These results confirm that, even if rapid SPS heating cycles are used, evolution of YAM and YAP phases into YAG phase is possible and exclude this hypothesis as the origin of the low transmission of YAG-B.

On the three powders, the influence of dwell time (between 5 and 60 min), applied load (between 30 and 70 MPa) and pressure application method was also studied. For YAG-B powder, the increase of pressure and/or dwell time led to only a slight increase of density, but a much more pronounced coloration of the samples, whereas, for YAG-S powder, no effect was observed, neither in terms of homogeneity of the samples nor in evolution of the microstructure. Increasing dwell and pressure in YAG-N samples led to transparent samples as well but the darkening was increased. Application of the pressure during the heating step or before dwell time did not lead to any significant difference in final density or visual appearance of the samples.

Even after investigation of the individual effect of various SPS parameters, YAG-B and YAG-S samples still reached moderate transparency. For YAG-B powders, samples were not fully densified, with the presence of minor secondary phases and sulphur, and exhibited a greyish coloration. Samples issued from YAG-S were inhomogeneous with an opaque centre and a transparent shell. Many reasons have been proposed to explain colorations and heterogeneity of translucent ceramics after sintering: graphite contamination [30], oxygen vacancies [18, 31], impurities [32], residual porosity [33], agglomerates [34], temperature or stress gradient during sintering [21, 35]. However, in our case, a negative effect of temperature or pressure gradients during SPS has to be ruled out, since the core and the outer part show the same microstructure.

YAG-N results were more positive, with transparent and homogeneous samples obtained after SPS treatments.

After the analysis of the SPS samples made with the three powders, there are still issues to understand the lack of transmission in YAG-B and YAG-S and improvements that can be made to YAG-N. Therefore, the effectiveness of other treatments was investigated: dispersion, LiF addition, air annealing and post-hipping in order to improve the optical transmission of the samples. For each powder, the choice of the treatments was oriented according to the possible issues detected after the SPS analysis.

(3) YAG-S improvement: Powder dispersion and post-treatments

Several authors have emphasized the influence of the dispersion of the ceramic powders on the optical transmission of sintered ceramics [13, 18]. Nanometric powders are particularly prone to agglomeration; during the calcination step, they agglomerate easily, leading to heterogeneous packing during pressing and potential formation of residual porosity during sintering. Moreover, agglomerates can lead to dislocations in compact samples and scattering centres in sintered ceramics [36].

In order to address the issue related to the critical influence of agglomeration in optical transmission, we aimed at developing YAG-S powder characterized by a finer and narrower particle size distribution. We dispersed the powder in water by means of strong ultrasonication with an external probe. This method gives generally better results and lower pollution degree than other routes such as ball milling [18]. After 45 min of dispersion (graph not shown here), a narrower grain size distribution is measured between 0.2 and 15 µm. Even if a partial re-agglomeration of the powder occurs after freeze drying, the size distribution (between 1 and 100 µm) appears narrower than the starting one. Dispersed powder was sintered with SPS at 1300 °C. Except for an increase of 4 % in the green density (indicating the partial efficiency of ultrasonic dispersion to break some agglomerates), no significant differences were observed on the sintering curve. A polished sample is shown in Fig. 4b and we observe that it presents a more homogeneous appearance, with a much less coloured core, so proving the influence of the agglomerates on the optical transmission.

To improve the optical transmission of the samples further, we evaluated the effect of a post-treatment. The efficiency of post annealing in air in eliminating oxygen vacancies engendered by vacuum sintering has been demonstrated elsewhere [15, 16]. This post-treatment should also remove any carbon contamination from the graphite SPS tooling. However, conditions of annealing are very sensitive: the temperature must be high enough to compensate for oxygen vacancies, but a too high temperature can also lead to pores or vacancies coalescence and consequently to a loss of the optical transmission [18]. In order to determine the optimal conditions of post-annealing, we tested different temperatures (from 900 to 1300 °C) and dwell times (from 1 to 24 h) on samples (obtained from dispersed powder) sintered by means of SPS. Annealing YAG-S samples at 1100 °C during 24 h (Fig. 4c) was more effective, as it resulted in much more homogeneous samples, even if still with residual coloration. Fig. 5 shows the optical transmission of YAG-S annealed samples. The TFT achieved was 40 % at 600 nm wavelength owing to the influence of the remaining darkening of the sample and the light absorption that it implies.

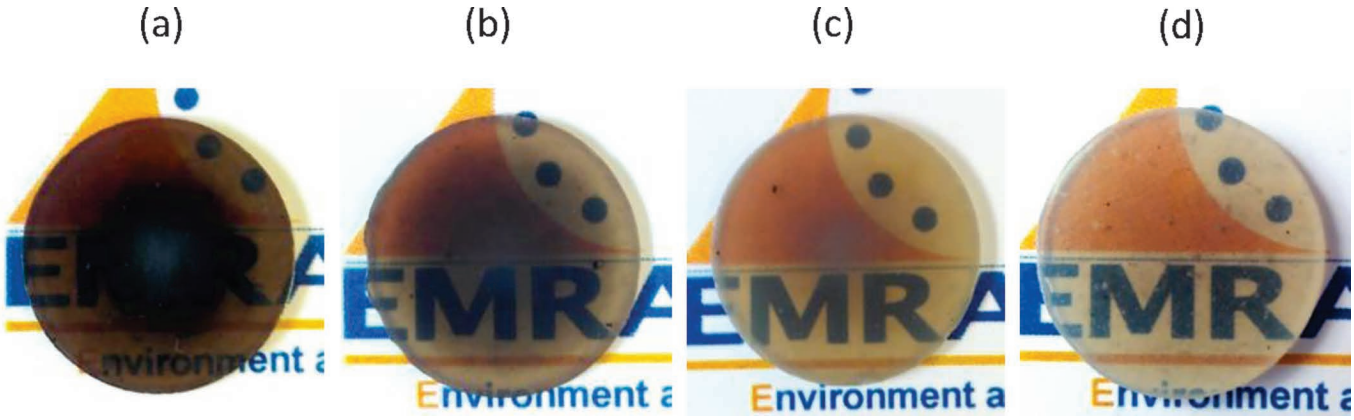

Fig. 4: Samples of YAG-S SPSed at 1300 °C without dispersion (a), dispersed with US and freeze-dried (b), after annealing at 1100 °C for 24 h (c) and after HIP at 1250 °C(d).

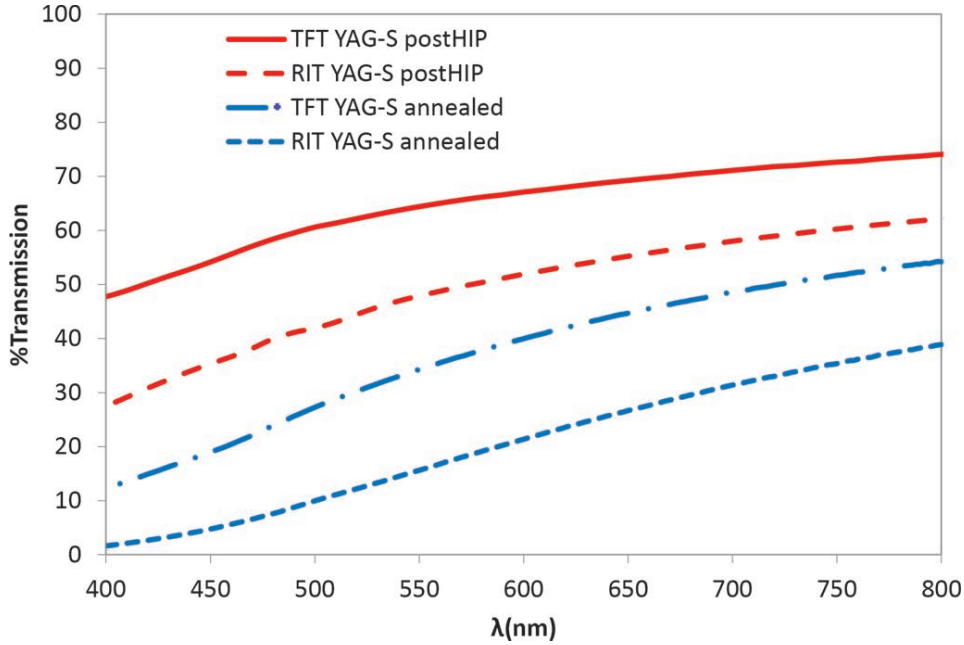

Fig. 5: Optical transmission (TFT and RIT) of 1-mm-thick SPSed samples obtained from YAG-S after annealing and after post-HIP.

Annealing in air allows oxygen vacancies and graphite removal but does not eliminate the remaining porosity. To address this issue, we performed post-treatments with Hot Isostatic Pressing (HIP) in an O_2/Ar atmosphere (20/80 vol%) on SPSed samples prepared from dispersed YAG-S powder. The cycle used for the HIP was a heating rate of 5 K/min up to 1250 °C with a pressure of 120 MPa and an isothermal step of 1 h. Annealing in oxygen, in addition to the application of higher pressures, could eliminate further oxygen vacancies and close the remaining porosity at the same time.

Fig. 4d shows a sample obtained after HIP. This sample presents 100 % density and a decrease in darkening. It can be observed that the sample is more homogeneous and transparent. No microstructural differences are observed after dispersion or post-treatments.

Optical transmission results of YAG-S after HIP are shown in Fig. 5 as well, where both Real In-line Transmission (RIT) and Total Forward Transmission (TFT) are presented. The HIP post-treatment has increased the transmission up to 48 % RIT and 59 % TFT at 600 nm.

YAG-S starting powder presents the highest agglomeration degree and the smallest particle size, so its compaction is inhomogeneous and probably leads to porosities inside the samples (not observed on SEM micrographs). Although dispersion decreases the agglomeration degree of this powder, it is not enough to obtain completely homogeneous samples. HIP post-treatment allowed more homogeneous and transparent samples to be obtained.

(4) YAG-B improvement: LiF addition

Dispersion of the starting powder, annealing and post-hipping on YAG-B samples was not very efficient and only a small improvement was achieved. Whatever annealing conditions we used, only a slight fading of the colour was obtained.

The inefficiency of these pre-treatments and post-treatments seems to point out the detrimental effect of the sulphur presence in the powder. To confirm this hypothesis, we explored the influence of LiF addition on the optical performance of YAG-B ceramics.

Lithium fluoride (LiF) is a commonly used additive to improve the optical transmission of spinel and YAG [19,37]. LiF melts at ~ 850 °C forming a liquid phase acting as a sintering aid. Li and F cations segregate at grain boundaries and increase grain-boundary mobility and surface diffusion. This promotes grain growth so it is mainly used on cubic ceramics where grain size does not directly affect transparency. A cleaning effect has also been attributed to LiF, and especially in SPS, it may help to get rid of carbon contamination caused by the graphite tooling. Moreover, LiF may also improve transparency by eliminating some other impurities such as S, Fe or Ca. Indeed, fluorine reacts with these impurity cations to form volatile compounds, the volatilization temperature of which is below the sintering temperature of the ceramic [32].

For improving both densification and optical transmission, high-purity LiF was added to the YAG-B powder. After testing of different amounts between 0.1 and 0.3 wt%, the optimal concentration of 0.2 % was selected. To get a good mixing between the LiF and YAG powders, lithium fluoride was added into a YAG aqueous suspension and ultrasonicated for 45 min. The mixture was then freeze-dried.

The sinterability of powder obtained in this way was investigated by means of SPS in the same conditions as those used for the non-doped powder. LiF-doped YAG-B powder showed a different sintering behaviour. The onset temperature was 1040 °C, 110 °C lower than non-doped YAG-B. Higher densities were attained at lower temperatures: for example at 1400 °C, 99 % vs. 94 %. Fig. 6a shows the microstructure of a sample sintered at 1450 °C: a significant increase in the grain size from 0.4 µm (non-doped sample: Fig. 3f) to around 6 µm (LiF-doped sample) can be observed, confirming the dramatic effect of LiF addition on grain growth. XRD measurement shows that the sample is pure YAG phase, indicating the correct stoichiometry of elements in the starting powder and the effect of LiF to complete transformation of intermediate phases (YAP and YAM) into YAG.

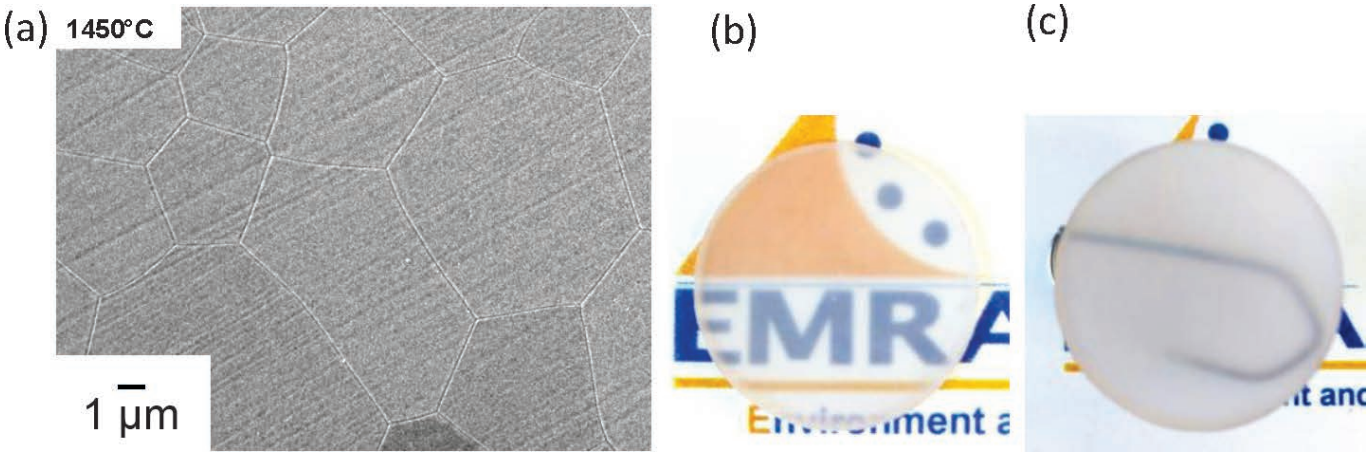

Fig. 6: Scanning electron micrograph (a) and images of 0.2%LiF-doped YAG-B SPSed sample (1450 °C, 50 MPa) placed on the text (b) and 15 mm above it (c) (1 mm thick).

Concerning the visual aspect of the sample (Fig. 6b and c), LiF addition has also a remarkable effect on YAG-B, as the sample shows a homogeneous and colourless aspect. In Fig. 6b, the sample placed on the text shows a transparent appearance. However, transparency of the same sample placed 1.5 cm above the text (Fig. 6c) appears to be very low, owing to strong light scattering. These differences agree with the optical transmission curves in Fig. 7, where a large discrepancy between TFT and RIT values is observed. Different sintering conditions were tested (temperature, pressure and dwell time), without decrease of the light scattering.

Similarly, no improvement of the in-line transmission was observed in any tested annealing conditions, suggesting that light scattering is not caused by oxygen vacancies. Different reasons might be proposed to explain this lack of transparency: residual porosities (not observed by SEM), LiF trapping on grain boundaries and/or triple points (ICP and XPS analysis on the samples have in fact revealed some traces of lithium and fluorine, but these are too low to be observed with SEM or detected in EDX analysis).

Finally, we also considered the residual amount of sulphur present in the LiF-doped YAG-B sample. We observed that the sulphur content of YAG-B is lower after SPS (150 ppm). LiF addition promotes a further decrease down to 40 ppm, but this content might be sufficient to explain the lack of transparency.

(5) YAG-N improvement: annealing

We observed that YAG-N samples were quite transparent after SPS, with only a slight darkening, certainly related to oxygen vacancies or/and carbon contamination. The best optical transmission was obtained for a sample sintered at 1500 °C (Fig. 8a), which achieved values of transmission of 64 % TFT and 59 % RIT at 600 nm, as we can observe in Fig. 9.

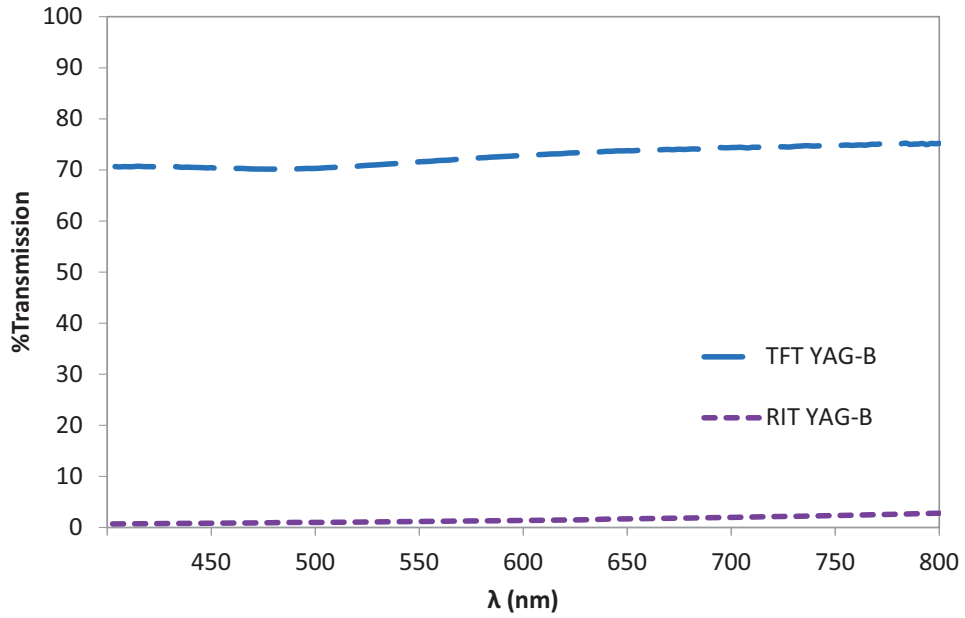

Fig. 7: Optical transmission (TFT and RIT) of 1-mm-thick SPSed samples obtained from YAG-B (doped with 0.2 % LiF).

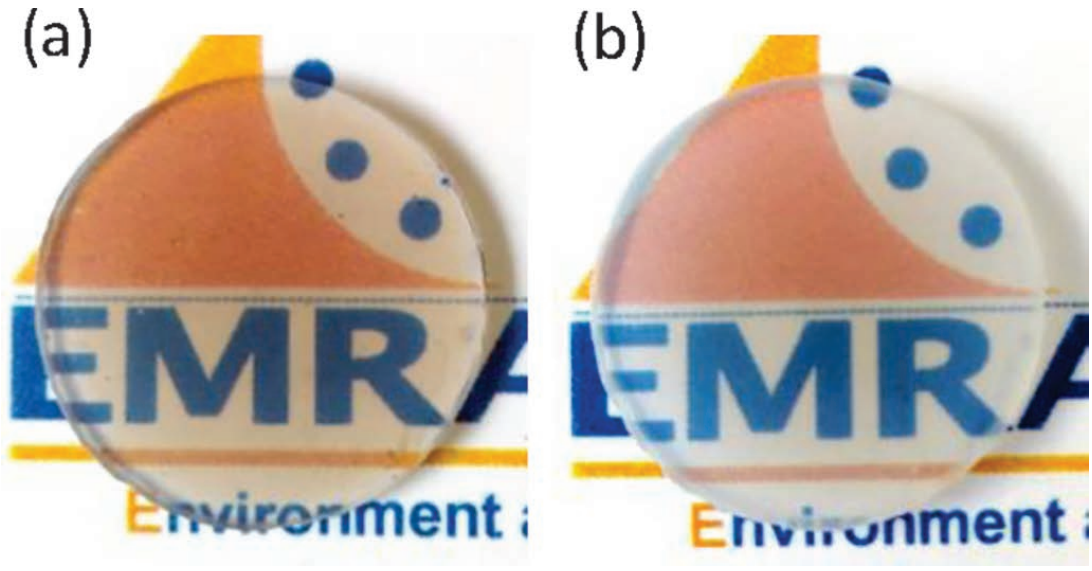

Fig. 8: Images of a 1-mm-thick YAG-N ceramic sintered in SPS (1500 °C, 50 MPa), before (a) and after annealing at 1150 °C (b).

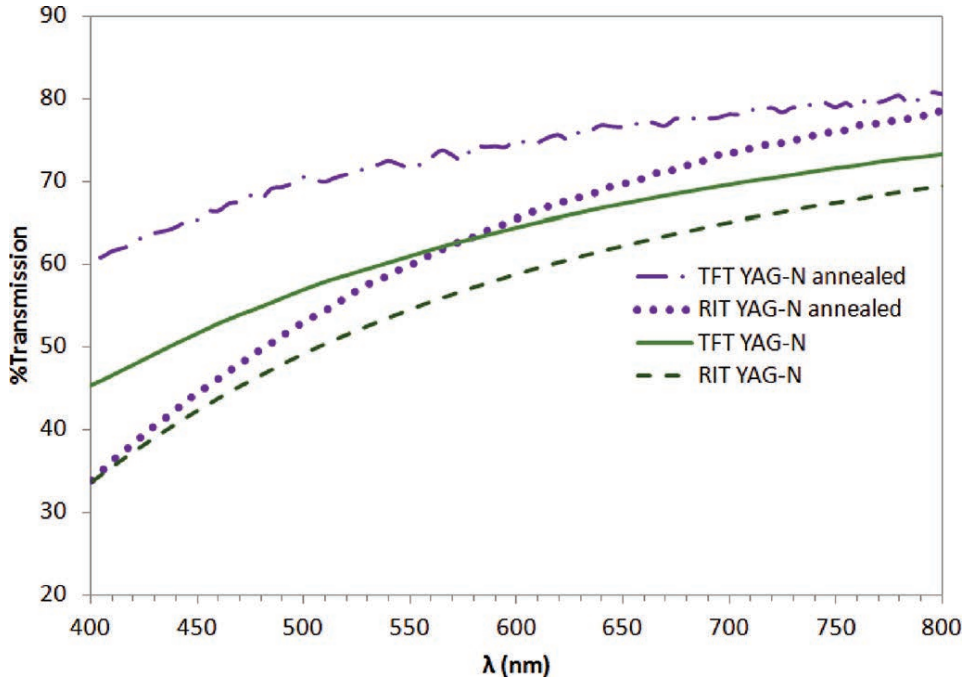

Fig. 9: Optical transmission (TFT and RIT) of 1-mm-thick SPSed samples obtained from YAG-N before and after annealing at 1150 °C.

Different annealing conditions were tested to remove the darkening of the samples. The better results were obtained after annealing in air at 1150 °C for 12 h (Fig. 8b). The optical transmission of a YAG-N annealed sample is presented in Fig. 9 and compared to the results before annealing. Both TFT and RIT values are high: at 600 nm, RIT is 66 % and TFT 75 %, which are close to the highest values of SPSed non-doped YAG samples reported in the literature [4, 13, 18, 30].

IV. Conclusions

This study compares the behaviour of three YAG powders sintered by means of spark plasma sintering. Sintering behaviour and final optical transmission are highly influenced by the powder properties. Pre- and/or post-treatments have to be adapted to each powder according to their physico-chemical characteristics. Both low agglomeration degree and homogeneous particle size distribution are found to be crucial to achieve high transmission values in the visible range. Annealing in air, applied in optimized conditions, reduces oxygen vacancies and carbon contamination, and consequently increases transparency. The presence of intermediate phases in the starting powder, even in large quantities, can be tolerated: indeed, it is shown that these phases can transform into YAG phase, even with such a rapid sintering technique as SPS. However, the presence of impurities, like sulphur, in the produced ceramics, even in an amount as low as 40 ppm, leads to a diminution of transparency. Best in-line transmission of 1-mm-thick sample after sintering at 1500 °C and annealing in air at 1150 °C for 12 h reaches 66 % (measured at 600 nm), a high value for spark-plasma-sintered non-doped YAG powder.

Acknowledgments

The authors thank the Walloon Region (Belgium) and the ESF (First-DOCA) for the financial support. This research used resources of the Electron Microscopy Service and XPS facilities of SIAM platform, both located at the University of Namur (Belgium).

References

1 Krell, A., Hutzler, T., Klimke, J., Potthoff, A.: Fine-grained transparent spinel windows by the processing of different nanopowders, *J. Am. Ceram. Soc.,* **93**, 2656 – 2666, (2010).

2 Morita, K., Kim, B.-N., Yoshida, H., Hiraga, K.: Spark plasma sintering condition optimisation for producing transparent $MgAlO_4$ spinel polycristal, *J. Am. Ceram. Soc.,* **92**, 1208 – 1216, (2009).

3 Sokol, M., Kalabukhov, S., Dariel, M.P., Frage, N.: High-pressure spark plasma sintering (SPS) of transparent polycrystalline magnesium aluminate spinel (PMAS), *J. Eur. Ceram. Soc.,* **34**, 4305 – 4310, (2014).

4 Chaim, R., Kalina, M., Shen, J.Z.: Transparent yttrium aluminum garnet (YAG) ceramics by spark plasma sintering, *J. Eur. Ceram. Soc.,* **27**, 3331 – 3337, (2007).

5 Ba, X., Li, J., Pan, Y. *et al.*: Comparison of aqueous- and non-aqueous-based tape casting for preparing YAG transparent ceramics, *J. Alloy. Compd.,* **577**, 228 – 231, (2013).

6 Goldstein, A., Krell, A.: Transparent ceramics at 50: Progress made and further prospects, *J. Am. Ceram. Soc.,* **99**, 3173 – 3197, (2016).

7 Kim, B.-N., Hiraga, K., Morita, K. *et al.*: Effects of heating rate on microstructure and transparency of spark-plasma-sintered alumina, *J. Eur. Ceram. Soc.,* **29**, 323 – 327, (2009).

8 Stuer, M., Zhao, Z., Aschauer, U., Bowen, P.: Transparent polycrystalline alumina using spark plasma sintering: Effect of mg, Y and La doping, *J. Eur. Ceram. Soc.,* **30**, 1335 – 1343, (2010).

9 Wang, S.F., Zhang, Y., Luo, D.W. *et al.*: Transparent ceramics: Processing, materials and applications, *Prog. Solid State Ch.,* **41**, 20 – 54, (2013).

10 Liu, J., Shen, Z., Yao, W. *et al.*: Visible and infrared transparency in lead free bulk $BaTiO_3$ and $SrTiO_3$ nanoceramics, *Nanotechnology*, **21,** (2010).

11 Krell, A., Klimke, J., Hutzler, T.: Transparent compact ceramics: Inherent physical issues, *Opt. Mater.,* **31**, 1144 – 1150, (2009).

[12] Liu, J., Yao, W., Kear, B., Ak, M.: Microstructure and IR transmittance of yttria-magnesia (50:50 vol%) nano-composites consolidated from agglomerated and ultrasonic horn treated nano-powders, *Mater. Sci. Eng. B,* **171**, 149 – 154, (2010).

[13] Suarez, M., Menendez, J.L., Torrecillas, R.: Transparent yttrium aluminium garnet obtained by spark plasma sintering of lyophilized gels, *J. Nanomater.,* (2009).

[14] Bernard-Granger, G., Benameur, N., Guizard, C., Nygren, M.: Influence of graphite contamination on the optical properties of transparent spinel obtained by spark plasma sintering, *Scripta Mater.,* **60**, 164 – 167, (2009).

[15] Kodera, Y., Hardin, C.L., Garay, J.E.: Transmitting, emitting and controlling light: Processing of transparent ceramics using current-activated pressure-assisted densification, *Scripta Mater.,* **69**, 149 – 154, (2013).

[16] Palmero, P., Bonelli, G., Fantozzi, G. *et al.*: Surface and mechanical properties of transparent polycristalline YAG fabricated by SPS, *Mater. Res. Bull.,* **48**, 2589 – 2597, (2013).

[17] Boulesteix, R., Maitre, A., Baumard, J.F., Rabinovitch, Y., Reynaud, F.: Light scattering by pores in transparent Nd:YAG ceramics for lasers: Correlations between microstructure and optical properties, *Opt. Express,* **18**, 14992 – 15002, (2010).

[18] Spina, G. *et al.*: Transparent YAG obtained by spark plasma sintering of coprecipitated powder. influence of dispersion route and sintering parameters on optical and microstructural characteristics, *J. Eur. Ceram. Soc.,* **32**, 2957 – 2964, (2012).

[19] Frage, N., Kalabukhov, S., Sverdlov, N. *et al.*: Effect of the spark plasma sintering (SPS) parameters and LiF doping on the mechanical properties and the transparency of polycrystalline Nd-YAG, *Ceram. Int.,* **38**, 5513 – 5519, (2012).

[20] Liu, W. *et al.*: Synthesis of Nd:YAG powders leading to transparent ceramics: The effect of MgO dopant, *J. Eur. Ceram. Soc.,* **31**, 653 – 657, (2011).

[21] Grasso, S., Hu, C., Maizza, G., Kim, B.-N., Sakka, Y.: Effects of pressure application method on transparency of spark plasma sintered alumina, *J. Am. Ceram. Soc.,* **94**, 1405 – 1409, (2011).

[22] An, L., Ito, A., Goto, T.: Two-step pressure sintering of transparent lutetium oxide by spark plasma sintering, *J. Eur. Ceram. Soc.,* **31**, 1597 – 1602, (2011).

[23] Powell, R.C., Physics of Solid-State Laser Materials. AIP Press, Springer-Verlag New York, Inc. New York, 1998

[24] Esposito, L., Piancastelli, A., Bykov, Y. *et al.*: Microwave sintering of Yb:YAG transparent laser ceramics, *Opt. Mater.,* **35**, 261 – 265, (2013).

[25] Pradhan, A.K., Zhang, K., Loutts, G.B.: Synthesis of neodynium-doped yttrium aluminum garnet (YAG) nanocrystalline powders leading to transparent ceramics, *Mater. Res. Bull.,* **39**, 1291 – 1298, (2004).

[26] Guesic, J.E., Marcos, H.M., Van Uitert, L.G.: Laser oscillations in Nd-doped yttrium aluminum, yttrium gallium and gadolinium garnets, *Appl. Phys. Lett.,* **4**, 182, (1964).

[27] Palmero, P., Esnout, C., Montanaro, L., Fantozzi, G.: Influence of the co-precipitation temperature on phase evolution in yttrium-aluminium oxide materials, *J. Eur. Ceram. Soc.,* **25**, 1565 – 1573, (2005).

[28] Apetz, R., Bruggen, M.P.: Transparent alumina. A light scattering model, *J. Am. Ceram. Soc.,* **86**, 480 – 486, (2003).

[29] Lee, S.-H., Kochawattana, S., Messing, G.L.: Solid-state reactive sintering of transparent polycrystalline Nd:YAG ceramics, *J. Am. Ceram. Soc.* **89**, 1945 – 1950, (2006).

[30] Frage, N., Kalabuknov, S., Sverdlov, N., Ezersky, V., Dariel, M.P.: Densification of transparent yttrium aluminum garnet (YAG) by SPS processing, *J. Eur. Ceram. Soc.,* **30**, 3331 – 3337, (2010).

[31] Lu, Z. *et al.*: Effect of air annealing on the color center in $Yb:Y_3Al_5O_{12}$ transparent ceramics with MgO as sintering additive, *Opt. Mater.,* **47**, 292 – 296, (2015).

[32] Rubat du Merac, M., Kleebe, H.-J., Müller, M., Reimanis, I.: Fifty years of research and development coming to fruition; unraveling the complex interactions during processing of transparent $MgAl_2O_4$, *J. Am. Ceram. Soc.,* **96**, 3341 – 3365, (2013).

[33] Pabst, W., Hostasa, J., Esposito, L.: Porosity and pore size dependence of the real in-line transmission of YAG and alumina ceramics, *J. Eur. Ceram. Soc.,* **34**, 2745 – 2756, (2014).

[34] Aman, Y., Garnier, V., Djurado, E.: Influence of green state processes on the sintering behaviour and the subsequent optical properties of spark plasma sintered alumina, *J. Eur. Ceram. Soc.* **29**, 3363 – 3370, (2009).

[35] Marlot, C.: YAG transparent ceramics processing: Co-precipitation synthesis and SPS, in French, Ph.D. Thesis, Université de Bourgogne, Dijon, 2013.

[36] Gong, H. *et al.*: Fabrication and laser performance of highly transparent Nd:YAG ceramics from well-dispersed $Nd:Y_2O_3$ nanopowders by freeze-drying, *J. Nanopart. Res.,* **13**, 3853 – 3860, (2011).

[37] Meir, S., Kalabukhov, S., Froumin, N., Dariel, M.P., Frage, N.: Synthesis and densification of transparent magnesium aluminate spinel by SPS processing, *J. Am. Ceram. Soc.,* **92**, 358 – 364, (2009).